Ion acceleration in the magnetic nozzle of an ECR thruster: Comparison of experimental measurements with a quasi 1D kinetic model

BARCELO RENACIMIENTO HOTEL, SEVILLE, SPAIN / 14 – 18 MAY 2018

S. Correyero[1], **J. Jarrige**[2], **D.Packan**[2], **E. Ahedo**[1]
[1]Equipo de Propulsión Espacial y Plasmas, Universidad Carlos III de Madrid, Leganés, Spain,
[2]ONERA, The French Aerospace Laboratory, Palaiseau, Paris, France,
Email:scorreye@uc3m.es.

KEYWORDS:

Magnetic nozzle, acceleration, Laser induced Fluorescence, Langmuir probe, kinetic modelling, ambipolar potential, magnetized expansion, electron cyclotron resonance

ABSTRACT:

This paper presents experimental results on the magnetic nozzle of the 50 W Electron Cyclotron Resonance (ECR) thruster of ONERA, consisting of a 27 mm diameter ECR cavity and a fully divergent magnetic nozzle, created by a Neodymium permanent magnet. The diagnostics installed are a cylindrical Langmuir probe to measure plasma potential, plasma density and electron temperature, and a Laser Induced Fluorescence set-up to measure the mean ion kinetic energy. Both the ion velocity and plasma potential profiles seem to be independent of the mass flow rate when normalized with the electron temperature estimated at the sonic transition of the plasma flow. This sonic transition appears to be slightly shifted downwards of the thruster exit. Results are compared with a supersonic collisionless kinetic 1D model where electron dynamics account for magnetic mirror effects and potential barriers, while ions are treated as a fluid cold species.

1 INTRODUCTION

During the past years, several authors have contributed to the physical understanding of different mechanisms involved in the magnetic nozzle expansion, such as plasma detachment, formation of ambipolar electric field, magnetic thrust, etc [1–4]. However, hypotheses on electron dynamics have been found to be crucial for characterizing the ion velocity profile. For instance, isothermal electrons lead to unbounded ion acceleration, and polytropic laws have demonstrated a limited valid range. In this context, a kinetic steady-state quasi 1D model was developed in Ref. [5] in order to determine self-consistently the axial evolution of the ambipolar electric potential and the electron and ion distribution functions of a fully magnetized plasma expansion.

Contrary to the commonly used polytropic laws, the model in [5] does not assume an expansion coefficient, but instead accounts for magnetic mirror effects and potential barriers to determine the electron velocity distribution function. The model determines the finite potential drop in the magnetized expansion, which for cold ions, only depends on the ion to electron mass ratio.

On the experimental side, ONERA has been developing an Electron Cyclotron Resonance (ECR) thruster during the past years composed of an ECR coaxial cavity followed by a divergent magnetic nozzle [6]. In order to investigate the ion acceleration and electron dynamics, an experimental set-up has been carried out at ONERA, where Langmuir probes have been used to characterize the evolution of the plasma potential, plasma density and electron temperature along the axis of the magnetic nozzle, and a Laser Induced Fluorescence (LIF) diagnostic has been employed to determine the mean ion velocity in the thruster exit plane and along the center line of the expansion [7].

In the work presented here, the kinetic model in [5] has been adapted to compare the solution with the experimental data along the magnetic nozzle obtained at ONERA.

This paper is organized as follows: Section 2- explains the set-up developed at ONERA and presents the main experimental results. Section 3- describes the model used to predict the plasma properties along the expansion. Finally, section 4- compares the experimental data with the theoretical model and section 5- concludes the main results of the research.

2 EXPERIMENTAL SET-UP

2.1 The ECR thruster of ONERA

The experiments carried out in this work were performed along the magnetic nozzle of the permanent magnet version of ONERA's ECR thruster [6]. It has an axisymmetric geometry and it is composed of a coaxial plasma source cavity of dimensions $L_\mathrm{s} = 15$ mm and $R_\mathrm{s} = 13.5$ mm followed by a divergent magnetic nozzle.

The inner conductor has a diameter of 1.7 mm, and

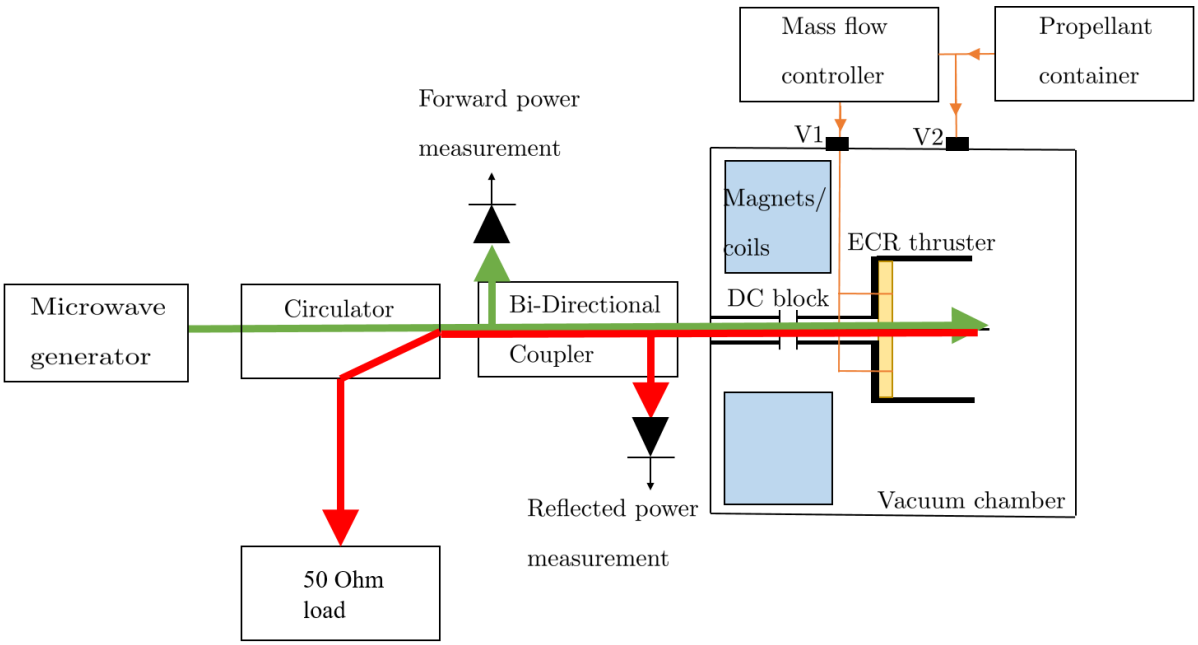

Figure 1: Schematic of the thruster and subsystems in the vacuum setup

ends 5 mm outside the thruster. The thruster walls are made of Aluminum while the antenna is made of stainless steel. The back of the source is limited by a dielectric backplate made of boron nitride. The thruster is electrically isolated by an in-line microwave component called Direct Current Blocker (DC block), which allows the thruster to be electrically floating. The propellant is injected at the back plate of the source through two holes of 1 mm diameter located symmetrically at two mid-points of the source radius. An external magnetic field is applied by means of a permanent magnet.
The microwave power is injected by means of a solid state amplifier from *Kuhne Electronic*. It is constituted by a signal generator (between 2.3 and 2.6 GHz) and a linear amplifier, and the maximum power it can deliver is around 100 W. The power is transmitted by a 50 Ohm coaxial cable, whose losses have been measured using a vector network analyzer. The output of the generator is connected directly to a circulator with a 50 Ohm load, which allows the reflected power to be absorbed and dissipated in the load. Subsequently and before entering the feedthrough, the power line contains a bi-directional coupler connected to two different diodes that are in charge of measuring the forward and reflected power at this point of the line. Figure 1 shows an schematic of the the microwave power line set-up.

2.2 Diagnostics

In order to obtain longitudinal profiles of the ion acceleration and plasma properties along the magnetic nozzle expansion, two different diagnostics were installed: Laser Induced Fluorescence (LIF) optical set-up and cylindrical Langmuir probes.
The LIF calibration and specific details of the optical setup are explained in [7], as well as the main results from the LIF measurements presented in this work. The laser consists of a SDL-TC10 tunable laser diode with 20 mW of maximum output power and the frequency span for this measurements was 25 GHz, which allowed measuring axial ion velocities up to 20 km/s.

The laser was aligned with the thruster axis and injected through a lens of 25 mm diameter. The detection was composed of a 50 mm lens and a 200 μm optic fiber. The probed volume was around 1 mm diameter. The optics were installed 450 mm far from the measurement point, to avoid perturbation and intrusion in the plasma beam. The detection was installed with an angle of 35^o and a camera was fixed to the thruster to verify alignment between the laser and the detection. All optics were fixed to the vacuum chamber, and the thruster was moved using a 3D translation stage. With this setup, any point in the thruster source and along the plume could be measured. Figure 2 schematizes the set-up.

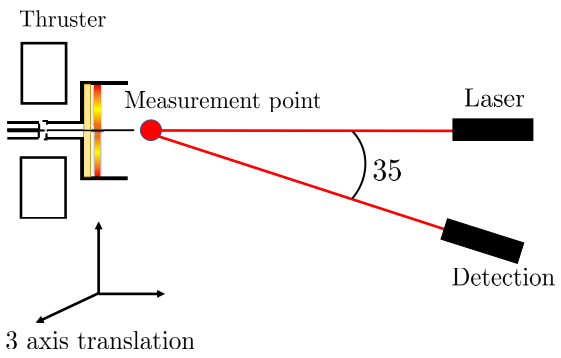

Figure 2: Schematic of optical LIF setup inside the vacuum chamber

A cylindrical Langmuir probe of 0.1 mm diameter and 6 mm length was placed in a complementary 2D translation stage, so it could operate at different longitudinal positions and be placed outside the optical line while performing the LIF acquisitions. The I-V characteristic curve was successfully obtained at different locations without perturbing significantly the thruster performance (from 75 to 250 mm from the thruster exit plane). The plasma potential was obtained from the inflection point of the I-V characteristic curve, and the electron energy distribution function (EEDF) was computed with the Druyvesteyn formula (Equation 1 [8], where $F(\epsilon)$ represents the EEDF, $g(\epsilon)$ the electron energy probability function (EEPF), m_e and q the electron mass and charge respectively and A the probe surface area). An effective electron temperature and density can be computed by taking the corresponding integrals of the EEDF, as it is shown in Equations 2 and 3. These formulas give reliable results when a magentic field is present if the condition $r_L >> r_s$ is satisfied, where r_L represents the electron Larmor radius or gyroradius and r_s the collecting area of the probe, taking into account the sheath expansion.

$$F(\epsilon) = g(\epsilon)\sqrt{\epsilon} = \frac{2\sqrt{2m_e\epsilon}}{q^3 A}\frac{d^2I}{dV^2} \qquad \text{(Eq. 1)}$$

$$n_e = \frac{2\sqrt{2m_e}}{|q|A}\int_0^{-\infty}\frac{d^2I}{dV^2}\sqrt{\frac{V}{|q|}}\,dV \qquad \text{(Eq. 2)}$$

$$T_e = \frac{4\sqrt{2m_e}}{3n_e A}\int_0^{-\infty}\frac{d^2I}{dV^2}\left(\frac{V}{|q|}\right)^{3/2}dV \qquad \text{(Eq. 3)}$$

2.3 Vacuum facility

The tests have been done at ONERA facilities, located in Palaiseau, Paris. The vacuum chamber, known as B09, consists of a cylindrical vessel with dimensions of 0.8 m diameter and 2 m long. The pumping is done by one primary pump, three Pfeiffer Hipace turbomolecular pumps, and one cryogenic pump, allowing to achieve a background pressure of 10^{-7} mbar and a Xenon pumping speed of 13000 l/s. Table 1 shows the measured chamber pressure when the thruster was operating at different mass flow rates.

2.4 Experimental results

This section presents the experimental results obtained at 30 W of absorbed power and 1, 1.5 and 2 sccm of Xenon. The coordinate z represents the distance to the thruster exit plane. The magnetic field intensity as a function of this distance is plotted in Figure 3.

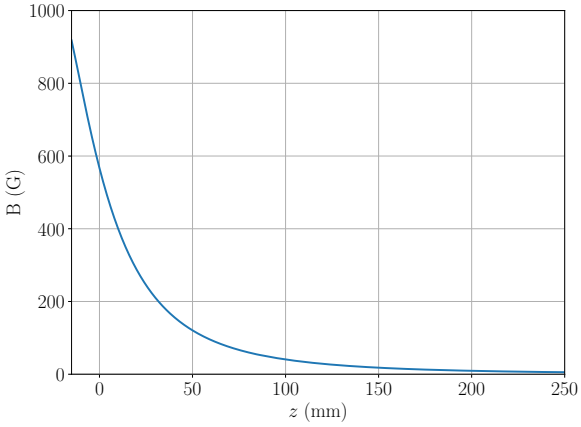

Figure 3: Magnetic field intensity along the thruster center line. $z = 0$ corresponds to the thruster exit plane.

Measurements with the Langmuir probe were taken from 75 mm to 250 mm downwards. It was not possible to place the probe closer to the thruster exit, since it is a very intrusive diagnostic, and it was disturbing the thruster performance. The estimated plasma potential, electron density and electron temperature along the expansion are shown in Figure 4 for the three different mass flow rates. The mean axial velocity is shown in Figure 5 for each case. As it can be seen, measurements were taken from the thruster exit plane to 115 mm downwards.

Xenon mass flow rate (mg/s)	Chamber pressure (mbar)
0.1	$2.8 \cdot 10^{-6}$
0.15	$3.5 \cdot 10^{-6}$
0.2	$3.7 \cdot 10^{-6}$

Table 1: Measured chamber pressure at three different xenon mass flow rate. The absorbed power was 30 W for all cases.

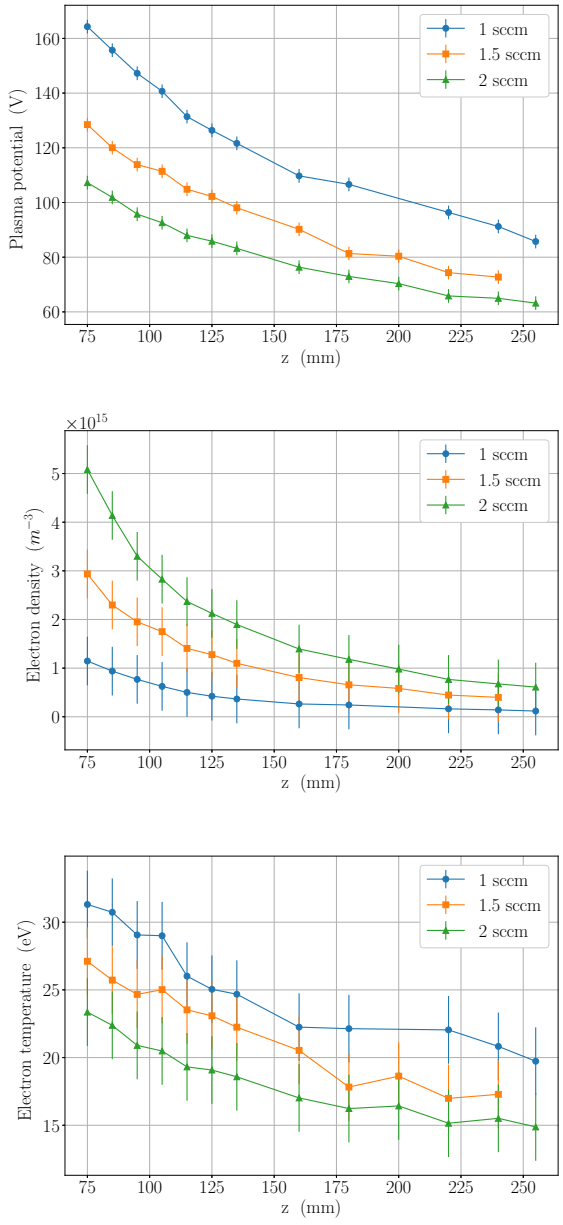

Figure 4: Longitudinal plasma properties: Plasma potential, electron density and electron temperature obtained with the Langmuir probe.

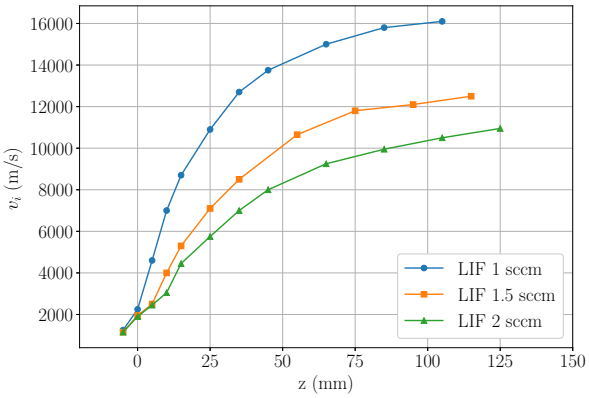

Figure 5: Mean axial ion velocity in the thruster axis obtained with the LIF optical set-up

Finally, the plasma potential measured with the Langmuir probe can be overlapped with the estimated potential from the LIF measurements assuming total ion energy is conserved. Figure 6 shows the plasma potential profile obtained combining both techniques.

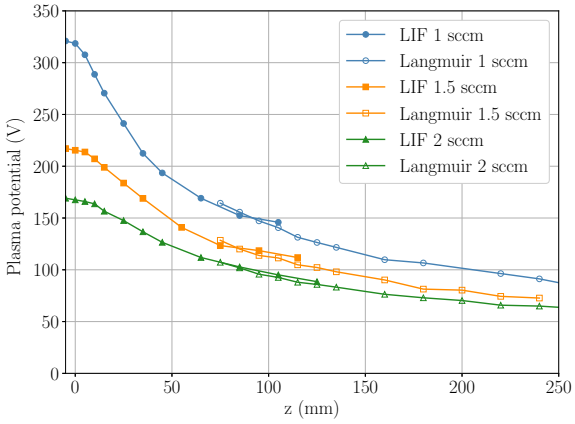

Figure 6: Plasma potential obtained with the Langmuir probe and LIF measurements assuming total ion energy is conserved.

Since there is an effective electron cooling along the expansion, an isothermal model would not be able to represent accurately the results. For this reason, and in order to reduce the number of assumptions and avoid fitting experimental polytropic coefficients,

a paraxial model is proposed which takes into account the depletion of the electron energy distribution function.

3 QUASI 1D EXPANSION MODEL

The model presented here is a variation of Martinez-Sanchez, Navarro and Ahedo's kinetic model detailed in [5]. Here, an externally applied magnetic field $B(z)$ vanishing at $B = +\infty$ and with a single maximum located at $z = 0$, generates a fully divergent magnetic nozzle that expands a plasma produced at $z = 0$. The model attempts to determine the quasi-1D, steady-state response of the plasma beam which is assumed collisionless.

In this approach, the dispersion in the ion velocity distribution function is neglected and ions are treated as a single cold species. Since the magnetic field is only divergent, all ions that leave the thruster would be accelerated downstream, so their motion is much simpler than for electrons. As well, ion total energy and ion flux are conserved along the expansion. This is shown in Equations 4 and 5, where m_i is the ion mass, u_i is the ion velocity, e is the elementary charge, and ϕ is the ambipolar electric potential, which is monotonically decreasing.

$$E_i = \frac{m_i u_i^2}{2} + e\phi = \frac{m_i u_{i0}^2}{2} + e\phi_0 \qquad \text{(Eq. 4)}$$

$$\frac{\Gamma_i}{B} = \frac{n_i u_i}{B} = \frac{n_{i0} u_{i0}}{B_0} \qquad \text{(Eq. 5)}$$

The electron population is modeled taking into account the effective potential barriers due to the magnetic mirror effect. The forward electron distribution f_{e+} is assumed Maxwellian upstream, at B_0, where plasma starts expanding, following the normalization $\int\int\int f_{e+} d^3w = n_{e0}$. f_{e+} is defined in Equation 1, where m_e is the electron mass, E_e is the electron energy, and n_{e*} and T_{e*} are reference parameters (the actual source density and electron temperature also involve the backward distribution).

$$f_{e+}(E_e) = n_{e*} \left(\frac{m_e}{2\pi T_{e*}} \right)^{3/2} \exp(-\frac{E_e}{T_{e*}}) \qquad \text{(Eq. 6)}$$

Electrons conserve their energy and magnetic moment, defined by equations 7 and 8.

$$E_e = \frac{m_e w_{e\parallel}^2}{2} + \frac{m_e w_{e\perp}^2}{2} - e\phi \qquad \text{(Eq. 7)}$$

$$\mu_e = \frac{m_e w_{e\perp}^2}{2B} \qquad \text{(Eq. 8)}$$

For each energy, there is a maximum magnetic moment μ_M where $w_{e\parallel} = 0$ at each location. Within this assumption, electrons from the plasma reservoir could belong to two different groups (free or reflected), while along the expansion there could be a population of electrons double-trapped in a region of the divergent nozzle. This population would be unconnected to the upstream source and it would be bouncing back and forward between the two spatial locations where their parallel energy vanishes. The double-trapped electrons could appear in the transient formation of the stationary flow [9] or due to infrequent electron collisions. We assume that the distribution function of these electrons has the same functional dependence than the one for electrons. Table 2 summarizes the main assumptions and characteristics of the model.

Quasi 1D model
Fully divergent
Collisionless
Quasineutral
Current-free
Electrons fully magnetized
Cold fluid ions
f_{e+} Maxwellian at $z = 0$
Monotonic plasma potential
Magnetic mirror effect and potential barriers
Populated regions of double-trapped electrons

Table 2: Main assumptions and characteristics of the model

Macroscopic variables are computed taking integral moments of the distribution function according to Equation 9, where the boundaries on the integration domain are set according to the type of electron (free, reflected, double-trapped).

$$\langle \chi_e \rangle = \frac{2\pi B\,(z)}{m_e^2} \int\int \chi_e(E_e, \mu_e) \frac{f_{e+}(E_e, \mu_e)}{|w_{e\parallel}|} dE_e d\mu_e \qquad \text{(Eq. 9)}$$

The self-consistent solution for the electric potential comes from solving the quasineutrality equation (Eq.10) with the current-free condition (Eq.11).

$$n_i(B(z), \phi(z)) = n_e(B(z), \phi(z)) \qquad \text{(Eq. 10)}$$

$$n_i u_i = n_e u_e \qquad \text{(Eq. 11)}$$

After normalizing Eq.10 and 11, the solution of the electric potential $\phi(B)$ depends on two parameters ϵ_i and M, defined in equations 12 and 13 , respectively.

$$\epsilon_i = \frac{E_i}{T_{e*}} \qquad \text{(Eq. 12)}$$

$$M = \frac{m_i}{m_e} \qquad \text{(Eq. 13)}$$

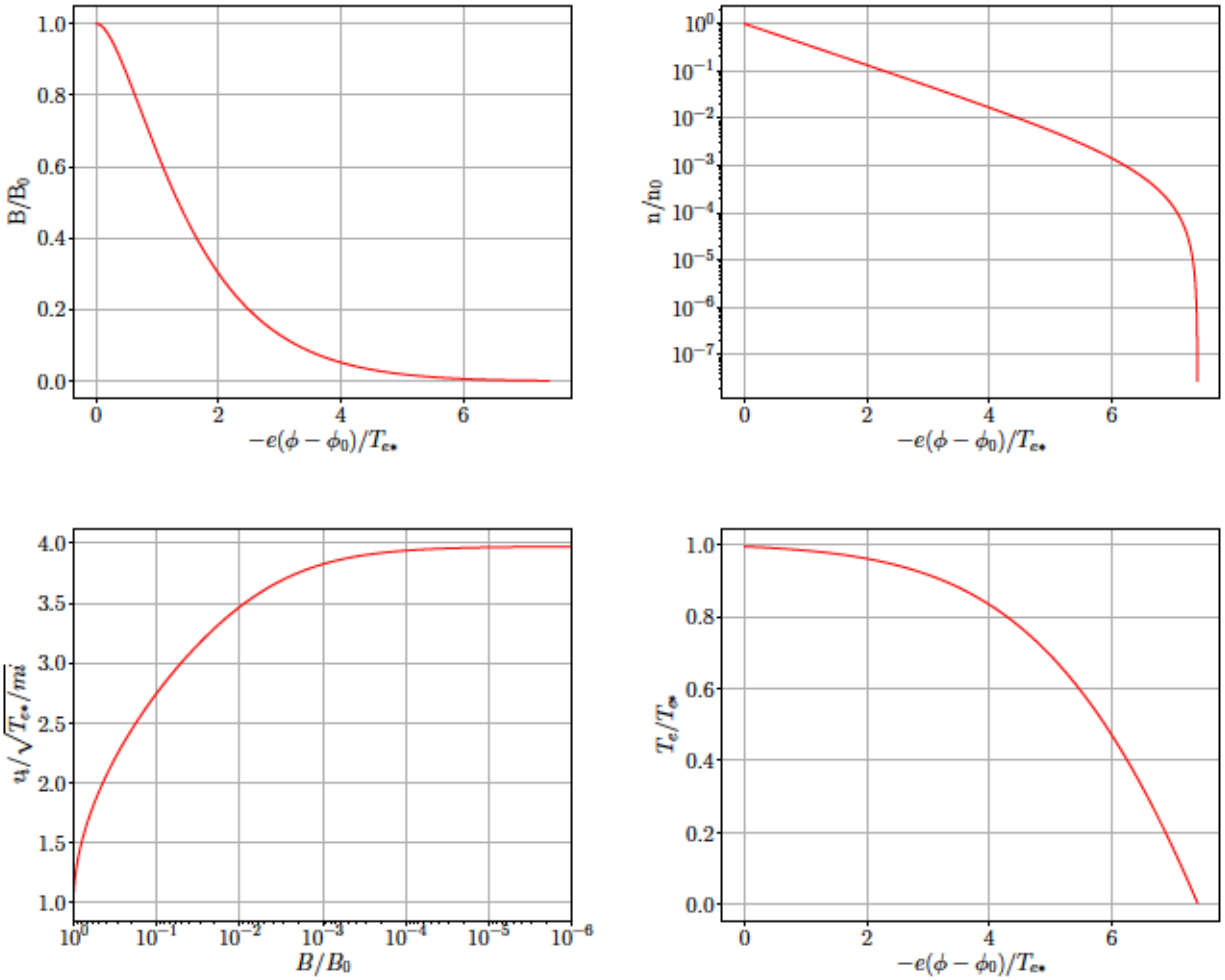

Figure 7: Model results for xenon ions and initial ion velocity equal to $\sqrt{T_{e*}/m_i}$

In this work, solutions have been obtained for initial ion velocities equal to $\sqrt{T_{e*}/m_i}$, and for Xenon ions ($M = 2.39 \cdot 10^5$). Figure 7 shows the solution $\phi(B)$ and the normalized plasma properties n/n_0, $v_i/\sqrt{(T_{e*}/m_i)}$, and T_e/T_{e*} for the mentioned parameters. The total potential drop obtained is $-e(\phi - \phi_0)/T_{e*} = 7.4$.

4 COMPARISON OF EXPERIMENTAL RESULTS WITH THE MODEL

This section presents the first comparison between the proposed analytical model and the experimental results. The longitudinal ion velocity and the plasma potential at the thruster axis can both be compared with the model, since the experimental data starts from the thruster exit plane.

Since the theoretical model proposed in this work is valid only for a collisionless supersonic expansion, the starting point corresponds to an ion velocity equals to $\sqrt{T_{e*}/m_i}$, so it is therefore necessary to identify the sonic transition in the experimental data, which is referred as $z = z_{s0}$ as follows. The region of minimum area (or maximum magnetic field) is not necessarily the "sonic" transition, since this point could be shifted due to ionization and/or diffusion processes [10]. Indeed, if the electron distribution function is non-isotropic already at the thruster exit, the temperature associated to the sonic transition is only the parallel component, so the results presented here should be corrected.

The reference temperature T_{e*} has been defined by fitting the experimental data with the quasi-1D model. This temperature can be seen in Table 3, with its corresponding sonic point in the expansion.

Xenon (mg/s)	T_{e*} (eV)	z_{s0} (mm)
0.1	45	7.4
0.15	27	11.8
0.2	19	12.5

Table 3: Estimated reference electron temperature at the sonic point and its location from the thruster exit plane

Figure 8 shows the comparison between the analytical model and the experimental data in terms of the mean ion velocity. The magnetic field has been normalized with its corresponding value at the sonic point $B_0 = B_{s0}$. As it can be seen, the three data sets normalized with their corresponding sound velocity $\sqrt{T_{e*}/m_i}$ follow the same tendency downwards of the "sonic" point, which is well represented by the model, but they follow different curves in the subsonic region.

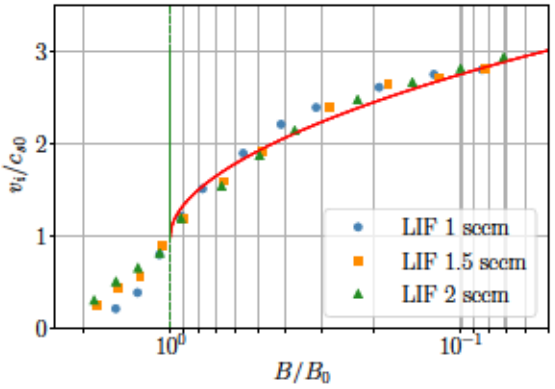

Figure 8: Normalized ion velocity from LIF measurements with $\sqrt{T_{e*}/m_i}$ and validity with the analytical model (red).

Figure 9 shows the measured plasma potential normalized with T_{e*} where the red line represents the model results. Again, if the plasma potential is normalized from the sonic point with a reference temperature T_{e*}, they follow the same curve independently of the mass flow rate. This is a very important result, since it reinforces the practicality of dimensionless 1D models. However, it is clear that the model should be improved to include ionization and diffusion processes, as well as anisotropy at the plasma reservoir, in order to properly identify the sonic transition in the expansion and avoid the calculation of a reference electron temperature T_{e*}.

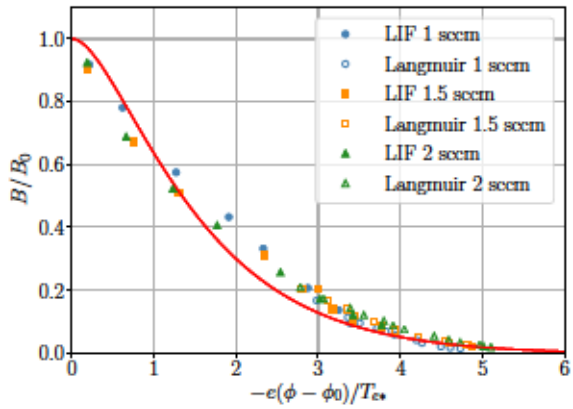

Figure 9: Normalized electric potential with the characteristic estimated T_{e*} and comparison with analytical model (red).

5 CONCLUSIONS

This paper presents experimental measurements of ion acceleration and plasma properties along the magnetic nozzle of the ECR thruster developed by ONERA. Langmuir probes and Laser Induced Fluorescence have been installed at ONERA facilities to determine the mean ion velocity, the plasma potential drop, electron density and electron temperature along the axis of the magnetic nozzle. The operating conditions were 30 W of absorbed power and 1, 1.5 and 2 sccm of Xenon.

The ion velocity profile and plasma potential have been normalized with a reference temperature T_{e*} and compared with a steady-state quasi 1D supersonic kinetic model. It has been found that the ion velocity and plasma potential profiles for different mass flow rates, follow the same curve when they are normalized and shifted to the sonic transition point.

A quasi 1D steady state model has been developed for a fully divergent magnetic field, assuming quasinuetrality and current-free expansion. The ion population is treated as a cold fluid species, while the electron distribution function is solved self-consistently accounting for magnetic mirror effects and potential barriers. Electrons are defined Maxwellian in the forward direction at the starting point of the expansion, while the complete population accounts for the backward and forward distribution, and allows regions of double-trapped electrons. A unique solution for the ambipolar potential profile has been found, which depends only on the ion to electron mass ratio and a parameter relating the ion energy with a reference temperature T_{e*}. A total potential drop of 7.4 T_{e*} has been calculated for Xenon.

Finally, the ion velocity and plasma potential profiles have been compared with the quasi-1D model. When normalizing the results, a reference tempera-

ture T_{e*} of 45 eV, 27 eV and 19 eV has been found for 1, 1.5 and 2 sccm, respectively. Despite the simple polytropic laws, the model presented here does not need to assume an expansion coefficient, and only depends on the ion to electron mass ratio. As a limitation when comparing with experimental results, the need of determining a reference electron temperature to define the sonic transition highlights the importance of obtaining accurate experimental data.

As a next step in this research, the model must be improved to determine consistently the sonic transition of the expansion, and justify the normalization presented in this work. A first modification would be to incorporate electron temperature anisotropy in the plasma source, this is, modifying the definition of the electron distribution at the plasma reservoir. A more complete simulation should include collisions and diffusion processes in the near plume region.

6 ACKNOWLEDGMENTS

This work was made in the framework of project MINOTOR that has received funding from the European Union's Horizon 2020 research and innovation programme under grant agreement No 730028. This work was additionally supported by the Spanish R D National Plan (Grant No. ESP2013-41052-P).

7 REFERENCES

[1] Arefiev, A. V. and Breizman, B. N., "Ambipolar acceleration of ions in a magnetic nozzle," *Physics of Plasmas*, Vol. 15, No. 4, 2008, pp. 042109.

[2] Ahedo, E. and Merino, M., "Two-dimensional supersonic plasma acceleration in a magnetic nozzle," *Physics of Plasmas*, Vol. 17, No. 7, 2010, pp. 073501.

[3] Longmier, B. W., Bering III, E. A., Carter, M. D., Cassady, L. D., Chancery, W. J., Díaz, F. R. C., Glover, T. W., Hershkowitz, N., Ilin, A. V., McCaskill, G. E., et al., "Ambipolar ion acceleration in an expanding magnetic nozzle," *Plasma Sources Science and Technology*, Vol. 20, No. 1, 2011, pp. 015007.

[4] Takahashi, K., Charles, C., and Boswell, R. W., "Approaching the theoretical limit of diamagnetic-induced momentum in a rapidly diverging magnetic nozzle," *Physical review letters*, Vol. 110, No. 19, 2013, pp. 195003.

[5] Martinez-Sanchez, M., Navarro-Cavallé, J., and Ahedo, E., "Electron cooling and finite potential drop in a magnetized plasma expansion," *Physics of Plasmas*, Vol. 22, No. 5, 2015, pp. 053501.

[6] Jarrige, J., Elias, P.-Q., Packan, D., and Cannat, F., "Characterization of a coaxial ECR plasma thruster," *44th AIAA Plasmadynamics and Lasers Conference*, 2013, p. 2628.

[7] Jarrige, J., Correyero-Plaza, S., Elias, P.-Q., and Packan, D., "Investigation on the ion velocity distribution in the magnetic nozzle of an ECR plasma thruster using LIF measurements," Tech. rep., IEPC-2017-382, 2017.

[8] Druyvesteyn, M. and Penning, F. M., "The mechanism of electrical discharges in gases of low pressure," *Reviews of Modern Physics*, Vol. 12, No. 2, 1940, pp. 87.

[9] Sánchez-Arriaga, G., Zhou, J., Ahedo, E., Martínez-Sánchez, M., and Ramos, J., "Kinetic features and non-stationary electron trapping in paraxial magnetic nozzles," *Plasma Sources Science and Technology*, Vol. 27, No. 3, 2018, pp. 035002.

[10] Burm, K., Goedheer, W., and Schram, D., "Mach numbers for gases and plasmas in a convergent-divergent cascaded arc," *Physics of Plasmas*, Vol. 6, No. 6, 1999, pp. 2628–2635.